Virginia Commonwealth University
VCU Scholars Compass

Physics Publications

Dept. of Physics

2009

Photoelectron imaging and theoretical investigation of bimetallic Bi1–2Ga–0–2 and Pb–1–4 cluster anions

M. A. Sobhy
The Pennsylvania State University

J. Ulises Reveles
Virginia Commonwealth University, jureveles@vcu.edu

Ujjwal Gupta
The Pennsylvania State University

Shiv N. Khanna
Virginia Commonwealth University, snkhanna@vcu.edu

A. W. Castleman Jr.
The Pennsylvania State University

Follow this and additional works at: http://scholarscompass.vcu.edu/phys_pubs

Part of the Physics Commons

Downloaded from

http://scholarscompass.vcu.edu/phys_pubs/194

Photoelectron imaging and theoretical investigation of bimetallic $Bi_{1-2}Ga_{0-2}^-$ and Pb_{1-4}^- cluster anions

M. A. Sobhy,[1] J. Ulises Reveles,[2] Ujjwal Gupta,[1] Shiv N. Khanna,[2] and
A. W. Castleman, Jr.[1,a)]

[1]*Departments of Chemistry and Physics, The Pennsylvania State University, University Park, Pennsylavnia 16802, USA*
[2]*Department of Physics, Virginia Commonwealth University, Richmond, Virginia 23284, USA*

We present the results of photoelectron velocity-map imaging experiments for the photodetachment of small negatively charged Bi_mGa_n ($m=1-2$, $n=0-2$), and Pb_n ($n=1-4$) clusters at 527 nm. The photoelectron images reveal new features along with their angular distributions in the photoelectron spectra of these clusters. We report the vertical detachment energies of the observed multiple electronic bands and their respective anisotropy parameters for the Bi_mGa_n and Pb_n clusters derived from the photoelectron images. Experiments on the $BiGa_n$ clusters reveal that the electron affinity increases with the number of Ga atoms from $n=0$ to 2. The $BiGa_2^-$ cluster is found to be stable, both because of its even electron number and the high electron affinity of $BiGa_2$. The measured photoelectron angular distributions of the Bi_mGa_n and Pb_n clusters are dependent on both the orbital symmetry and electron kinetic energies. Density-functional theory calculations employing the generalized gradient approximation for the exchange-correlation potential were performed on these clusters to determine their atomic and electronic structures. From the theoretical calculations, we find that the $BiGa_2^-$, $Bi_2Ga_3^-$ and $Bi_2Ga_5^-$ (anionic), and $BiGa_3$, $BiGa_5$, Bi_2Ga_4 and Bi_2Ga_6 (neutral) clusters are unusually stable. The stability of the anionic and neutral Bi_2Ga_n clusters is attributed to an even-odd effect, with clusters having an even number of electrons presenting a larger gain in energy through the addition of a Ga atom to the preceding size compared to odd electron systems. The stability of the neutral $BiGa_3$ cluster is rationalized as being similar to $BiAl_3$, an all-metal aromatic cluster. © *2009 American Institute of Physics*. [DOI: 10.1063/1.3069295]

I. INTRODUCTION

Information on the structure and energetics of clusters is used to gain insight into the microscopic details of intermolecular interactions.[1,2] Metal clusters have been the subject of intensive experimental and theoretical studies due to their importance in fundamental and practical applications, with particular focus on the dependence of their electronic structure, chemical and catalytic activities on the atomic structure, and cluster size.[3–5] Main-group elements play an important role in semiconductor materials, and there has been extensive spectroscopic and theoretical works on these compounds in the solid state for band gap determination.[6] Due to their technological and fundamental importance, mixed clusters of semiconductors formed of groups III and V elements have also been extensively studied, and the evolution of their electronic properties as a function of size and composition has been investigated.[7–13] Unlike transition-metal clusters, which exhibit very high densities of low-lying electronic states due to the d orbitals, main-group metal clusters including dimers have discernible low-lying electronic states because of the bonding through open np shells.[14] Also, among the important members in the main group metals are tetravalent elements, which provide an interesting case for understanding chemical bonding.[15] The ability of carbon to form multiple bonds and a variety of structures as rings and chains lays the foundation for organic chemistry.[16,17] Other tetravalent elements as Si, Ge, Sn, and Pb show different bonding properties that significantly vary with the atomic number, where Si is found to form a network diamond structure, while Pb exhibits a close-packed metallic lattice.[18] The trend toward metallic packing with higher atomic number results in part from the reduced s-p hybridization caused by the increase in the s-p valence electron energy differences.[19]

Negative ion photoelectron spectroscopy has been an important tool for studying metal clusters due to the favorable combination of mass selectivity and flexible transition selection rules.[20] Another valuable technique is photoelectron imaging, which has been recently applied to investigate negative ions.[21] Photoelectron imaging simultaneously measures the kinetic energies and the angular distributions of the detached electrons, thus providing information about the partial wave functions composition of the orbital through which the photodetachment process occurs.[22] In the present study, we report the results of the photoelectron imaging experiments on small semiconductorlike clusters made of gallium and bismuth, groups III and V elements, respectively. The photoelectron images of $BiGa_n^-$ and $Bi_2Ga_n^-$ clusters ($n=0-2$), obtained using 527 nm and the stability of the $BiGa_n$ and Bi_2Ga_n series are investigated. Also, small Pb_n^- clusters ($n=2-4$) were studied using the same wavelength. The re-

a)Electronic mail: awc@psu.edu.

corded images show distinct variation in the angular distribution of the electronic bands arising from the change in the cluster size. There are several studies on Pb_n^- clusters using negative ion photoelectron spectroscopy.[23–25] However, to the best of our knowledge, this is the first time that anionic gallium-bismuth and Pb_n^- clusters have been studied using photoelectron imaging.

II. EXPERIMENTAL AND COMPUTATIONAL METHODS

The experimental setup is briefly discussed, and further details can be found in a previous work.[26] The binary metal target is made from a mixture of nearly equal weights of bismuth and gallium melted and molded in the form of a 0.25 in. diameter rod. The second harmonic of a neodymium-doped yttrium aluminum garnet laser (532 nm, 20 mJ/pulse) is focused on the rotating and translating target. The bimetallic clusters are formed through the expansion of He at 90 psi pressure from a pulsed valve running at 10 Hz into a vacuum chamber. A cold cluster beam is formed by supersonic expansion of the vaporized metal-carrier gas mixture through an expansion nozzle and collimated through a skimmer. The clusters are then perpendicularly extracted and accelerated into a Wiley–McLaren time-of-flight mass spectrometer.[27] Ions are detected with a high gain microchannel plate detector (MCP) that can be placed off-axis to allow photofragmentation studies by analyzing the daughter fragments using a single-stage reflectron mass spectrometer.[28] Upon arrival to the center of the velocity-map photoelectron imaging spectrometer, the mass-selected negatively charged clusters are intercepted with the output of the second harmonic of a neodymium:yttrium lithium fluoride (Nd:YLF) laser at 527 nm (2.35 eV), which is linearly polarized parallel to the detector surface. The detached electrons are focused through the use of appropriate voltages on the imaging plates and projected on a position-sensitive MCP coupled to a phosphor screen. In order to reduce the background, the potential difference across the imaging MCPs is pulsed from 1.2 to 1.8 kV for an interval of 300 ns to coincide with the arrival time of the photodetached electrons.[28] The images are acquired over 30 000–40 000 experimental cycles through a charge coupled device camera. The three-dimensional distributions are reconstructed from the photoelectron images using the BASEX program[29] The velocity distribution and photoelectron energy spectra are then obtained from the reconstructed images. The anisotropy parameter β is determined from the photoelectron angular distributions obtained from the images and the photoelectron differential cross-section equation,

$$I(\theta) = (\sigma/4\pi)[1 + \beta P_2(\cos\theta)], \tag{1}$$

where σ is the total detachment cross section, θ is the angle between the laser polarization and the electron velocity vector, and $P_2(\cos\theta)$ is the second-order Legendre polynomial equal to $[(3\cos^2\theta - 1)/2]$.[30] The measured electron affinities (EAs) and anisotropy parameter values are reproducible among different sets of experiments. The electron kinetic energies are calibrated using the EAs of Ag, Cu, and Bi atomic ions.

To aid in the assignment of the experimentally measured photoelectron spectra, and to investigate the stability of the clusters, we carried out first-principles electronic structure investigations on the anion and neutral forms of Bi_mGa_n ($m = 0-2$; $n = 1-6$) and Pb_n ($n = 1-4$) clusters. These calculations were performed within the density functional formalism (DFT) and employed the Perdew *et al.*[31] generalized gradient approximation (GGA). The electronic orbitals and eigenstates were determined by using a linear combination of Gaussian atomic type orbitals molecular orbital approach. The actual calculations were carried out using the DEMON2K software.[32] For Ga we employed the double-ζ valence plus polarization (DZVP) basis set optimized for GGA exchange-correlation functionals.[33] The Bi and Pb atoms were described respectively using the 23 and 22 electron scalar relativistic effective core potentials proposed by Metz *et al.*,[34] in combination with the correlation consistent aug-cc-pVDZ valence basis sets.[35] The A2 auxiliary function set for Ga and the GEN-A2* auxiliary function set for Bi and Pb were used. The exchange-correlation potential was calculated from the orbital density.

In order to determine the ground state geometries, the configuration space was sampled by starting from several initial configurations, optimizing the geometry in redundant coordinates without symmetry constraints,[36] and where after the resulting ground states were characterized via a frequency analysis. The molecular geometries and orbitals were plotted using the SCHAKAL[37] and MOLEKEL[38] software, respectively. In general, we found the Bi_mGa_n clusters to have many isomers, some of them being very close in energy. In this study, we report the isomers that are within a range of less than 0.10 eV higher in energy with respect to the ground state. In order to test the reliability of our computational method, we calculated several properties of the Ga, Bi, and Pb atoms and clusters. For the Ga atom, the EA was calculated as 0.26 eV in agreement with the experimental values that range from 0.30 ± 0.15 to 0.430 ± 0.03.[39] For the Bi atom, we correctly predicted the ground state spin multiplicity of the neutral species as a quartet, the anion as a triplet, and the EA was calculated to be 0.85 eV in good agreement with the experimental value of 0.942 eV.[40] The Bi_2 was calculated as a singlet with a bond length of 2.67 Å and a binding energy of 2.74 eV. The determined bond length is in excellent agreement with the experimental value of 2.66 Å,[41] while the calculated binding energy overestimates the experimental value of 2.04 eV,[42] as higher binding energies are generally known to occur in DFT.[43] To further benchmark our methodology, we calculated the geometries of pure neutral and anionic Ga_n clusters, ($n = 1-6$) where previous calculations exist by Zhao *et al.*[44] and Song and Cao.[45] We were able to reproduce the reported ground states geometries and multiplicities, while our calculated vertical detachment energies (VDEs) reproduced the experimental and theoretical trends with fair agreement. For the Pb_n clusters ($n = 2-4$), the calculated optimized geometries and binding energies are in excellent agreement compared with the GGA theoretical calculations of Rajesh *et al.*[46] Finally, our calculated VDEs are in very good agreement compared to the experimental values
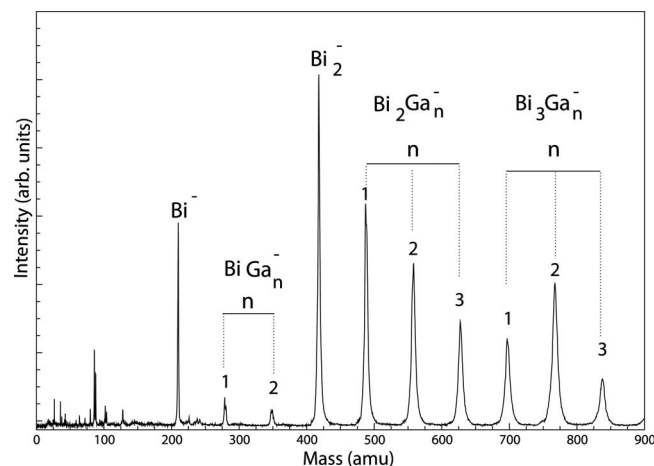
FIG. 1. The time-of-flight mass spectrum of bimetallic cluster anions produced by laser ablation of a mixed Bi/Ga target is shown. The $Bi_2Ga_n^-$ ($n=1-3$) clusters are more abundant compared to the $BiGa_n^-$ ($n=1-2$) and $Bi_3Ga_n^-$ ($n=1-6$) clusters.

reported in this study, and with those measured by Ganteför *et al.*[23] and Ho *et al.*[25]

FIG. 2. (Color online) The raw and reconstructed photoelectron images of Bi^- atomic ion and binary $BiGa_n^-$ with $n=1,2$ clusters recorded at 527 nm are depicted in columns A and B, respectively. The symbols X and A denote the electronic transitions from the anionic ground state to the first and second excited states of the neutral, respectively. The arrow indicates the polarization direction of the laser electric field, which is vertical in the image plane. The reconstructed images are drawn to a larger scale than the corresponding raw photoelectron image to emphasize the electronic band features, but they have the correct relative size among themselves. The charge density of the HOMO and HOMO-1 along with their symmetry and percentage of atomic composition are shown in column C.

III. RESULTS AND DISCUSSION

The time-of-flight mass spectrum of bismuth and gallium bimetallic cluster anions is shown in Fig. 1. In this study, we investigate the photoelectron spectra and atomic structures of Bi_mGa_n clusters with one and two Bi atoms. The Bi_3Ga_n series is studied in a separate work.[47] The $Bi_2Ga_n^-$ with $n=1-3$ clusters are more abundant compared to the $BiGa_n^-$ with $n=1-2$, and $Bi_3Ga_n^-$ with $n=1-3$ clusters. The photoelectron images of atomic Bi^- and $BiGa_n^-$ $n=1,2$ clusters recorded at 527 nm (2.35 eV) are depicted in Fig. 2. The raw and reconstructed photoelectron images are shown in columns (A) and (B), respectively, where the laser polarization vector is coincident with the vertical axis of the images. The reconstructed images show better resolved features and qualitatively indicate the preferential orientation of the electronic bands in relation to the laser polarization. The highest occupied molecular orbital (HOMO) and HOMO-1 charge density plots along with the respective symmetry are shown in column (C) of Fig. 2. The measured detachment energies, the anisotropy parameters, and calculated detachment energies for the respective transitions are given in Table I.

The photoelectron image of the atomic Bi^- ion shows two electronic transitions marked X and A. The ground state of Bi^- is a spin triplet in a $^3P_2$ state and the removal of one electron results in a neutral either with spin quartet ($^4S_{3/2}$ state), or doublet ($^2D_{3/2}$ state) depending, respectively, on whether the electron is removed from the minority or majority spin state. The transition X corresponds to the quartet neutral ground state and results from the removal of one electron from a paired p-orbital. Our studies also indicate that the neutral spin doublet results form the removal of one of the unpaired p electrons in Bi^-, hence the transitions X and A can be regarded as resulting from two orthogonal p-orbitals. The electronic band X exhibits partial parallel distribution while band A is isotropic.
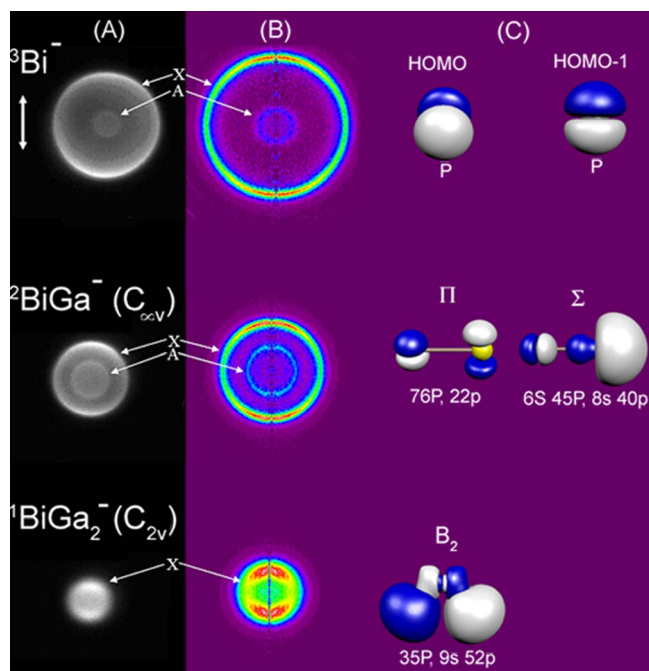
The EAs of the $BiGa_n$ clusters increase as the number of Ga atoms increase from 0 to 2 as seen from the progressive decrease in size of the electronic bands in the photoelectron images of $BiGa^-$ and $BiGa_2^-$ clusters. The ground state of $BiGa^-$ is a doublet and the HOMO and HOMO-1 are almost degenerate (energy difference ~ 0.03 eV), with Π and Σ symmetries, respectively, as shown in column (C) of Fig. 2. Column (C) also gives the percentage of s and p atomic composition of the molecular orbitals, with upper and lower case letters for Bi and Ga atoms, respectively. In $BiGa^-$ both HOMO and HOMO-1 have dominant p character although the HOMO-1 has partial atomic s orbital composition. The photoelectron angular distribution of transition X resulting from the detachment of the HOMO is partially parallel to laser polarization, while the electronic band A is nearly isotropic. The calculated vertical transition energy from the $BiGa^-$, which has a doublet ground state, to the neutral BiGa with a triplet ground state is 1.92 eV, reasonably close to the experimental value of 1.63 ± 0.1 eV. The vertical transition to the singlet state was not adequately described within the density-functional framework and is not reported here. There is only one accessible transition in the $BiGa_2^-$ cluster at the used photon energy and the calculated value of 2.33 eV matches the experimental finding of 2.17 ± 0.15 eV. The EA of the $BiGa_2$ cluster is significantly higher than that of BiGa as shown from the measured EAs as well as by the theoretical calculation results. As shown in Table I, the calculated

TABLE I. Relative energies (E_{rel}), experimental and theoretical VDEs to neutral states of $M \pm 1$, adiabatic EA, and calculated HOMO-LUMO gaps of the neutral and anionic BiGa$_n$ ($n=1-6$) clusters. The superscripts indicate the M spin multiplicity. All values are given in units of eV.

	$E_{\text{rel.}}$	Band	VDE exp.	β-parameter	VDE theo.	EA exp.	EA theo.	HOMO-LUMO gap
^{3}Bi$^-$		X	0.94 ± 0.1	0.52 ± 0.1	0.85	0.94	0.85	0.57
		A	2.11 ± 0.1	0.05 ± 0.1	2.33			
^{2}BiGa$^-$	0.0	X	1.63 ± 0.1	0.66 ± 0.15	1.92			0.12
		A	2.18 ± 0.1	0.18 ± 0.15				
	0.01	X			1.79			0.06
^{3}BiGa						1.5	1.71	0.72
^{1}BiGa$_2^-$	0	X	2.17 ± 0.15	0.35 ± 0.1	2.33			1.63
	0.09	X			2.38			1.63
^{2}BiGa$_2$	0.0					1.90	2.18	0.73
	0.08							0.35
^{2}Bi$_2^-$		X	1.20 ± 0.1	-0.2 ± 0.1	1.17			0.13
		A	1.96 ± 0.1	-0.7 ± 0.1	2.34			
		B	2.32 ± 0.1	-0.18 ± 0.1				
			2.33 ± 0.1	-0.06 ± 0.1				
			2.34 ± 0.1	0.06 ± 0.1				
^{1}Bi$_2$						1.00	1.10	1.99
^{1}Bi$_2$Ga$^-$		X	2.11 ± 0.1	0.22 ± 0.15	2.03			0.52
		A	2.32 ± 0.15	0.06 ± 0.15				
^{2}Bi$_2$Ga						1.95	1.90	0.60
^{2}Bi$_2$Ga$_2^-$	0.0	X	1.96 ± 0.1	-0.02 ± 0.15	2.12			0.50
		A	2.25 ± 0.1	0.45 ± 0.15	2.38			
	0.0	X			2.07			0.56
		A			2.49			
^{1}Bi$_2$Ga$_2$						2.00	1.78	0.90

EAs of BiGa$_2$ and BiGa are 2.18 and 1.71 eV, respectively. The BiGa$_2^-$ is also found to have a stable even electron count. The observed electronic band X results from detachment of HOMO of B_2 symmetry, which is predominantly composed of p orbitals with partial atomic s composition. The electronic band distribution is nearly isotropic with partial orientation parallel to the laser polarization.

Figure 3 depicts the optimized geometries of the ground state and low-lying energy isomers of the anionic and neutral BiGa$_n$ clusters with $n=1-6$ series. The clusters exhibit the lowest possible multiplicity, singlet and doublet for the even and odd electron systems, respectively, with the exception of BiGa, which has a triplet ground state. The Bi–Ga bond lengths in the anionic BiGa$_n$ clusters with $n \leq 2$ ranged from 2.59 to 2.68 Å, and are relatively smaller than those of the neutral clusters. For $n > 2$, the Bi–Ga bond in both anionic and neutral clusters ranged from 2.80 to 3.0 Å. The BiGa$_3$ cluster, however, presented Bi–Ga bond lengths of only 2.69 Å in a planar C_{2v} symmetry. At $n > 4$ the clusters favored compact structures, although the low-lying energy isomer of BiGa$_4^-$ also exhibits a compact structure in the triplet state. The BiGa$_5$ anion and neutral clusters show similar compact geometries, but while neutral BiGa$_5$ has C_s symmetry, the anionic cluster exhibits a nonsymmetric structure. For BiGa$_6$, the anionic low-lying energy isomer and the neutral ground state have similar geometries with the anionic ground state being more compact. In general, Bi tends to coordinate with mostly Ga atoms, which can be explained based on the larger experimental binding energy of the Bi–Ga dimer of 1.65 eV (Ref. 42) compared with Ga–Ga of 1.43 eV.[42]

The raw and reconstructed photoelectron images of Bi$_2$Ga$_n^-$ with $n = 0, 1, 2$ clusters are shown in Fig. 4. Three electronic transitions are observed for Bi$_2^-$ designated as bands X, A, and B, respectively, according to their increasing EAs. Both transitions X and B are nearly isotropic with slightly perpendicular orientation with respect to the laser polarization. Band B shows three peaks whose anisotropy parameters are slightly negative or close to zero, since isotropic distributions become dominant at very low electron kinetic energies.[22] Band A shows almost perpendicular orientation to the laser polarization. The transition of band X results from the HOMO mostly composed of p atomic orbitals and corresponds to the final neutral ground state $^1\Sigma_g^+$ of Bi$_2$, as discussed by Polak *et al.*[9] In our case, the calculated transition energy of 1.17 eV is in excellent agreement with the experimental value of 1.20 ± 0.1 eV (Table I). Transition from band A and B has been previously assigned[9] based on the ordering of spin-orbit states calculated by Balasubramanian *et al.*[48] to the triplet states $^3\Sigma_u^+ (1u)$ and $^3\Sigma_u^+ (0_u^-)$, respectively. We calculated only one triplet state for which the transition resulting from the HOMO-1, and with an energy of 2.34 eV that agrees with the transition energy of band B of 2.32 ± 0.1 eV.

The photoelectron binding energy spectra of the BiGa$_n^-$ $n = 1$, 2 and Bi$_2$Ga$_n^-$ $n = 1, 2$ clusters are shown in Fig. 5. The spectra are normalized and plotted on the same electron binding energy scale. The features in the spectra are labeled with the same letters used to mark the corresponding electronic bands in the photoelectron images of the respective species. The vertical dotted line marks the EA of the Bi
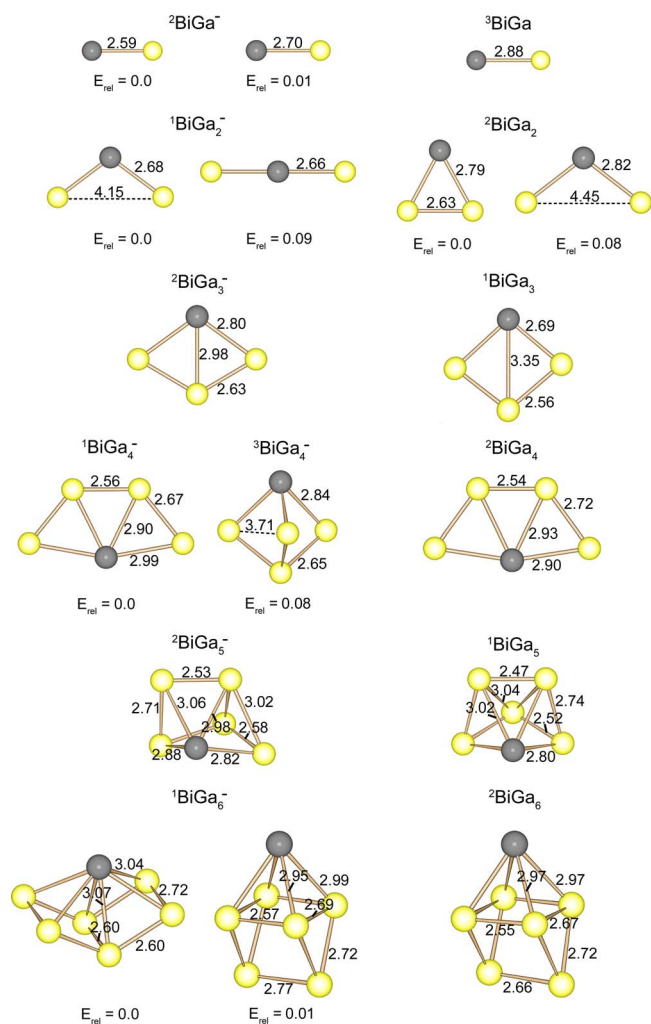
FIG. 3. (Color online) Optimized geometries of $BiGa_n(n=1-6)$ anionic and neutral clusters. Bond lengths are given in angstroms and the superscripts indicate spin multiplicity. The relative energies of the low lying energy isomers are given in units of eV. The gray circles correspond to Bi atoms, while the yellow circles represent Ga atoms.

FIG. 4. (Color online) The raw and reconstructed photoelectron images of the Bi_2^- dimer and binary Bi_2Ga_n with $n=1,2$ clusters recorded at 527 nm are depicted in columns A and B, respectively. The symbols X, A, and B denote the electronic transitions from the anionic ground state to the first and higher excited states of the neutral species. The HOMO and HOMO-1 charge density plots along with their respective symmetry and percentage of atomic composition are shown in column C. (See caption of Fig. 2 for more details.)

tial s orbital character. The calculated transitions of both the ground state and the nearly degenerated energetic isomer agree quantitatively with the experimental transitions (Table I).

The optimized geometries of the ground states and low-lying energy isomers of the anionic and neutral Bi_2Ga_n with $n=1-6$ series are shown in Fig. 6. All clusters show the lowest possible multiplicity. The Bi–Bi bond was found to be maintained at larger size, which can be explained based on the experimentally determined binding energy of the Bi–Bi

atom. The photoelectron image of the Bi_2Ga^- cluster in Fig. 4 shows two isotropic electronic bands corresponding to the two transitions X and A in the photoelectron spectrum in Fig. 5. Transition X arises from the HOMO of B_2 symmetry mainly of p orbital character and exhibit a nearly isotropic with slight parallel angular distribution. The photoelectron angular distributions in clusters and molecular species can be dependent on several parameters, for example, the electron kinetic energies and the symmetry of the orbital from which the electron is detached leading to deviations from the expected angular distributions for photodetachment from an atomic orbital. The calculated EA of Bi_2Ga_2 is slightly lower than that of the Bi_2Ga cluster. There are two accessible electronic transitions in the Bi_2Ga_2 cluster, where the lower binding energy band X appears as a faint halo in the photoelectron image in Fig. 4 and as a side peak in the photoelectron spectrum of the $Bi_2Ga_2^-$ cluster depicted in Fig. 5. The isotropic band X results from the detachment of the HOMO of B_1 symmetry, similar in shape to a d orbital. Band A has slight orientation parallel to the laser polarization and occurs from the detachment of HOMO-1 of B_2 symmetry with par-
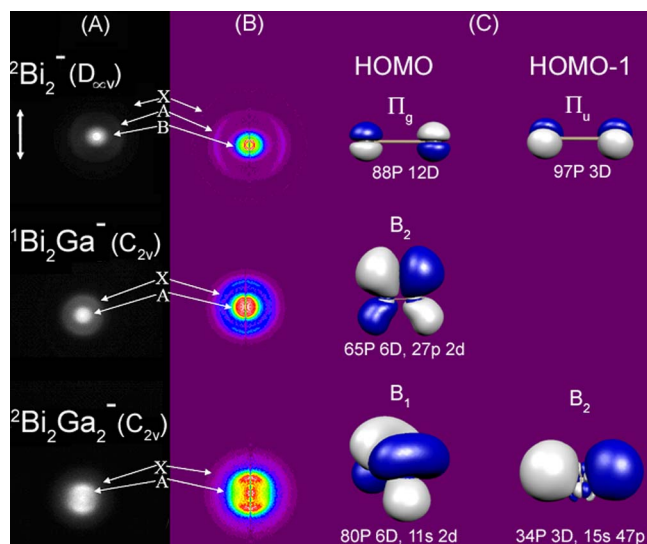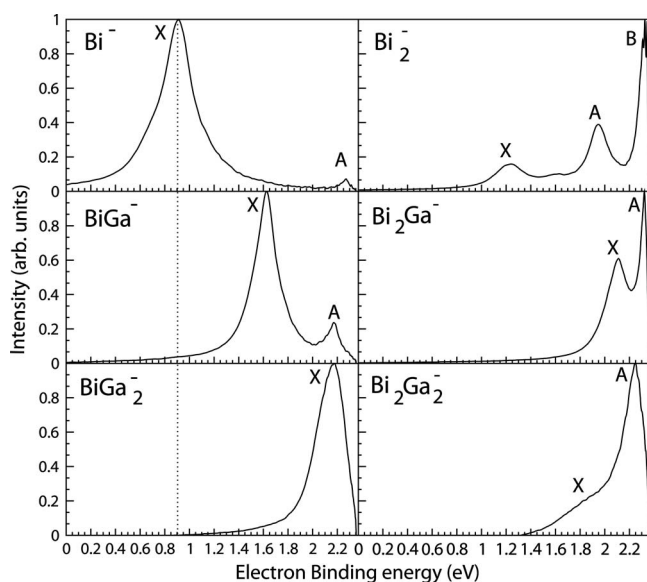

FIG. 5. The photoelectron energy spectra of $Bi_mGa_n^-$ cluster anions, where $m=1,2$ and $n=1,2$, obtained using photons of 527 nm wavelength. The spectra are normalized and plotted on the same energy scale. The dotted line, which denotes the EA of the Bi atomic ion, is drawn for comparison with the EAs of the $BiGa_n$ clusters.
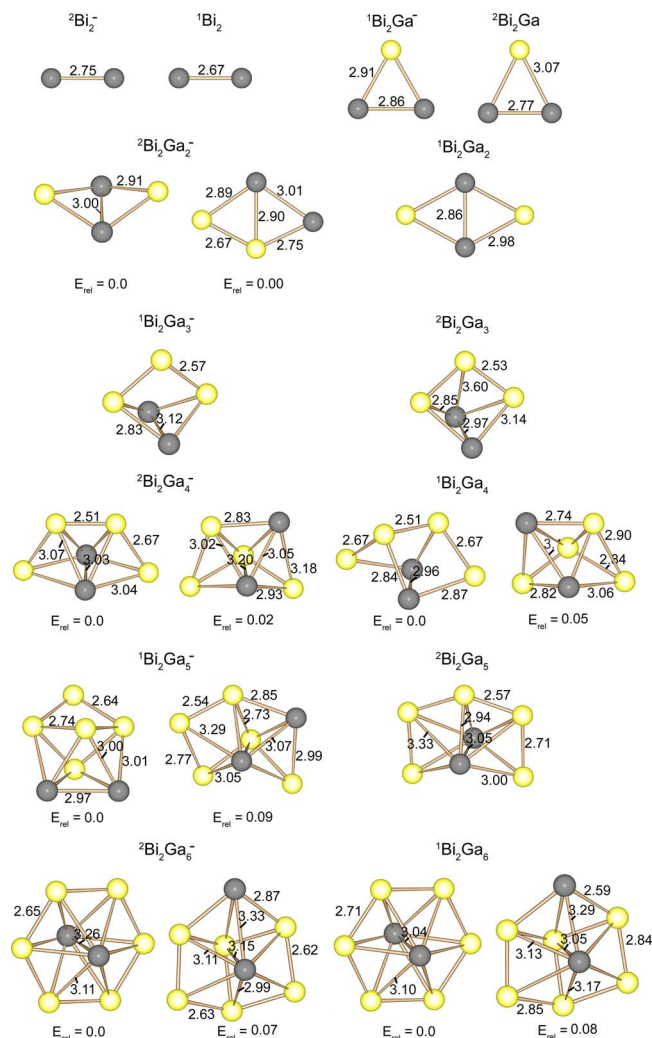
FIG. 6. (Color online) Optimized geometries of Bi_2Ga_n ($n=0–6$) anionic and neutral clusters. Bond lengths are given in angstroms and the superscripts indicate spin multiplicity. The relative energies of the low lying energy isomers are given in units of eV. The gray circles correspond to Bi atoms, while the yellow circles represent Ga atoms.

dimer of 2.04 eV (Ref. 42), which is higher than that of the Bi–Ga and Ga–Ga dimers. The Bi_2Ga neutral and anionic clusters show C_{2v} symmetries in which the Bi–Bi bond is stretched compared to the respective neutral and anionic Bi_2 dimers bond lengths. Although one anionic Bi_2Ga_2 isomer was found to have a nonplanar geometry with both Ga atoms in a bridge configuration, an energy-degenerate isomer exhibited a planar configuration in which both Ga_2 and Bi_2 dimers are bonded parallel to each other. The geometry of neutral Bi_2Ga_2 is similar to the anion cluster, but has a higher symmetry planar D_{2h} structure. Compact geometries were found for $n>3$, and in general two types of geometries were found. In the first type, which is present in most of the ground states, the Bi–Ga bonds are favored where the Ga atoms connects to the Bi_2 dimer. In the second type, the Ga atoms form clusters to which the Bi_2 dimer binds externally.

In order to investigate the stability of the anionic and neutral $BiGa_n$ and Bi_2Ga_n series, we calculated the gap between the HOMO and the lowest unoccupied molecular orbital [HOMO-LUMO gap (LUMO denotes lowest unoccu-

pied molecular orbital)], the EAs, and the energy gain ΔE_{Ga} when successive Ga atoms bind to Bi and Bi_2, respectively, $\Delta E_{Ga} = E(Bi_mGa_{n-1}) + E(Ga) - E(Bi_mGa_n)$. Here $E(Bi_mGa_n)$, $E(Bi_mGa_{n-1})$, and $E(Ga)$ are the total ground state energies of the Bi_mGa_n, Bi_mGa_{n-1} clusters, and that of the Ga atom. A large HOMO-LUMO gap is commonly used as an indicator of chemical stability, where the system resists both the change in the number of electrons and the deformation of the electronic cloud. In addition it should be noted that a cluster containing an odd number of electrons will generally have a zero HOMO-LUMO gap in a spin restricted calculation since the HOMO is singly occupied. In a spin-unrestricted approach, however, the up and down spin orbitals are allowed to have different spatial characters; the energy levels do not occur "in pairs" for the two spin components and a HOMO-LUMO gap does open up. For comparisons of HOMO-LUMO gap, we analyze variations between closed shell clusters only. Maxima in the EA among a series imply a special stability of the corresponding anionic species, while a large energy gain ΔE_{Ga} in the formation of a cluster from a stoichiometry with one less atom and a small gain in energy when one extra atom binds to the cluster attest for energetic stability. Figure 7 shows the HOMO-LUMO gaps and calculated ΔE_{Ga} of the anionic and neutral $BiGa_n$ and Bi_2Ga_n clusters, while the corresponding values are given in Table S1 in the supplementary material[49] of this article.

Inspection of Fig. 7 shows that $BiGa_2^-$, $Bi_2Ga_3^-$, and $Bi_2Ga_5^-$ (anionic), and $BiGa_3$, $BiGa_5$, Bi_2Ga_4 and Bi_2Ga_6 (neutral) clusters have higher ΔE_{Ga} than the neighboring clusters. These clusters also have significant HOMO-LUMO gaps. Additionally, the calculated EAs yield maxima for $BiGa_2$, Bi_2Ga_3, and Bi_2Ga_5 of 2.18, 2.64 and 2.32 eV, respectively as shown in Tables S2 and S3,[49] attesting for the stability of the corresponding $BiGa_2^-$, $Bi_2Ga_3^-$, and $Bi_2Ga_5^-$ anionic species. In order to examine the special stability of $BiGa_2^-$ we analyzed the electronic levels and the nature of the orbitals of Bi, and the molecular orbitals of Ga_2^- and $BiGa_2^-$ as shown in Fig. S1.[49] The neutral Bi atom has a quartet ground state with a $6p^3$ electronic configuration and three single occupied p levels. On the other hand, Ga_2^- is also a quartet state with three electrons of p character. The three p levels of Ga_2^- can then be considered to interact with the three empty levels of Bi forming covalent bonds and generating the $BiGa_2^-$ even electron system with a large HOMO-LUMO gap. Following the same principle, $BiGa_3$ is formed through the bonding interaction of $3p$ electrons from Bi and $3p$ electrons of Ga_3. In this case, the cluster acquires further stability as the p_z orbitals perpendicular to the plane of the molecule combine to form a delocalized π orbital, while the p_x and p_y orbitals are oriented radially toward the center of the ring, and tangentially around the ring, respectively, form two delocalized σ orbitals, as shown in Fig. S2.[49] Attesting for the delocalized nature of these orbitals, the $BiGa_3$ presented shorter Bi–Ga and Ga–Ga bonds than the rest of the series, as discussed above. In this way, $BiGa_3$ has features of an all-metal aromatic cluster in analogy to the recently reported $BiAl_3$ cluster.[50] Similarly, the stable $BiGa_5$ cluster could be regarded as an analog of $BiAl_5$,[50] which has a compact and symmetric structure. The electron energy levels and
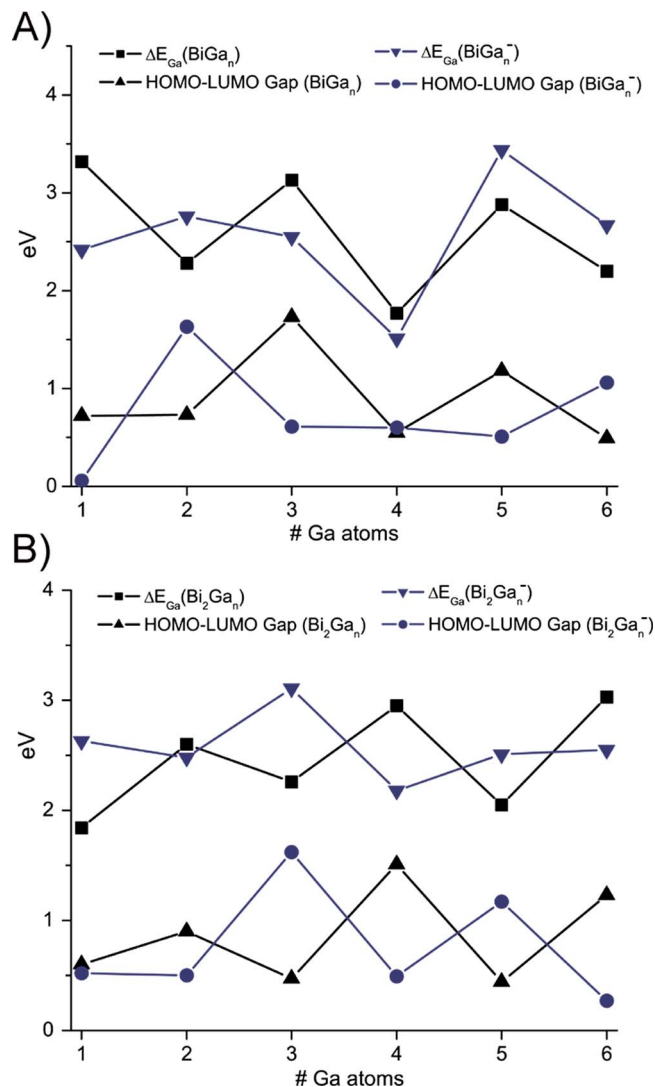
FIG. 7. (Color online) Calculated Ga gain energies (ΔE_{Ga}) and HOMO-LUMO gaps (in units of eV), of (a) the neutral and anionic $BiGa_n (n=1-6)$ clusters, and (b) the neutral and anionic $Bi_2Ga_n (n=1-6)$ clusters. Ga gain energies include zero point energy corrections.
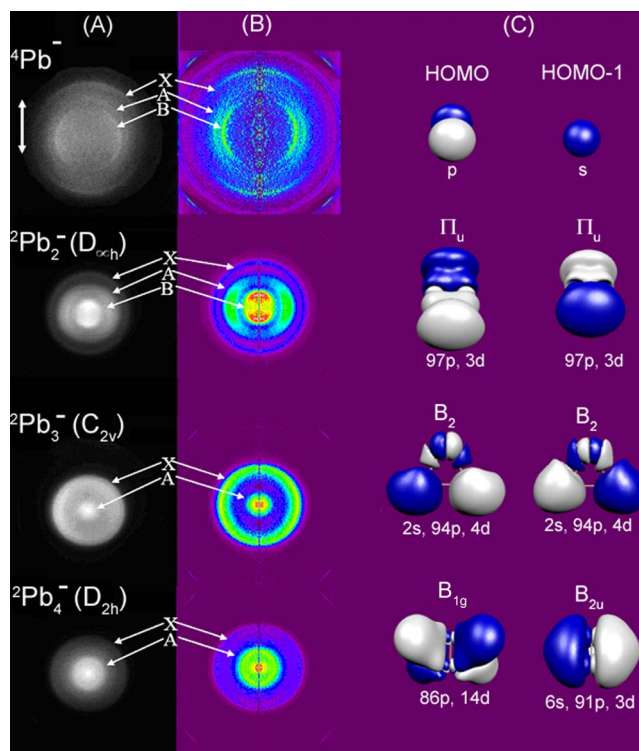

FIG. 8. (Color online) The raw and reconstructed photoelectron images of Pb_n^- clusters with $n=1-4$ recorded at 527 nm are depicted in columns A and B, respectively. The symbols X, A, and B denote the electronic transitions from the anionic ground state to the first and higher excited states of the neutral species. Column C depicts the charge density of the HOMO and HOMO-1, and their symmetry character and percentage of atomic orbital composition. (See caption of Fig. 2 for more details.)

molecular orbital isosurfaces are shown in Fig. S3.[49] The shapes of the orbitals suggest an electronic ordering of the types $1s^2$, $1p^6$, $1d^{10}$, and $2s^2$ reminiscent of a closed shell at 20 electrons.

An analysis of ΔE_{Ga} for the Bi_2Ga_n series in Fig. 7 shows an even-odd oscillation with respect to the number of Ga atoms. Previous studies of similar III-V clusters: $In_2P_3^-$,[51] $Ga_2As_3^-$,[52] and $Ga_2P_3^-$,[53] concluded that systems having an even number of electrons exhibit enhanced stability when compared with systems with an odd number of electrons. In the present study, we found that the enhanced stability of the neutral and anionic Bi_2Ga_n series can be explained by the same even-odd behavior.

The photoelectron images of Pb_n with $n=1-4$ clusters obtained using 527 nm are shown in Fig. 8. The photoelectron image of atomic Pb^- anion shows three transitions at this photon energy. The band of the ground state transition X is partially parallel while those of the two higher binding energy transitions A and B are partially perpendicular to the laser electric field. The angular distribution in transition X is

dependent on the kinetic energy of the detached electrons, where at high kinetic energies ~2 eV, transitions resulting from a p orbital can exhibit partial perpendicular distribution with respect to the laser field. The dependence of the anisotropy parameters for p-orbital detachment on the electron kinetic energy was demonstrated for atomic ions,[54] where near threshold the angular distribution is nearly isotropic; at ~1 eV β becomes ~ -1 (i.e., perpendicular distribution) then β increases to 2 (i.e., parallel distribution) by increasing the electron kinetic energy.[25] The photoelectron image of Pb_2^- has three accessible electronic transitions at this photon energy, where band X appears as an isotropic ring, while bands A and B show perpendicular and parallel distributions to the laser polarization, respectively. The measured detachment energies, anisotropy parameters, and the calculated detachment energies for the Pb_n^- clusters ($n=2-4$) are given in Table II. For Pb_2^- the symmetry of both the HOMO and HOMO-1 orbitals, shown in Fig. 8, is Π_u with the same partial atomic orbital composition of p and d orbitals. The transition of band X results from the HOMO and corresponds to the final neutral ground state $^3\Sigma_g^-$ of Pb_2, as discussed by Ho et al.[25] We calculated a transition energy of 1.56 eV in good agreement with the experimental value of 1.48 ± 0.1 eV (Table II). Transition from bands A and B has been previously assigned[25] based on the ordering of spin-orbit states calculated by Balasubramanian and Pitzer[55] to the triplet states $^3\Sigma_g^-$ (1_g) and $^3\Pi_u$ (2_u), respectively. In these works, two other transitions at slightly higher binding ener-

TABLE II. Experimental and theoretical VDE to neutral states of $M \pm 1$, adiabatic EA, and calculated HOMO-LUMO gaps of the neutral and anionic $Pb_n (n=1-4)$ clusters. The superscripts indicate the M spin multiplicity. All values are given in units of eV.

	Band	VDE exp.	β-parameter	VDE theo.	EA exp.	EA theo.	HOMO-LUMO gap
$^2Pb_2^-$	X	1.48 ± 0.1	-0.02 ± 0.15	1.56			0.05
	A	1.9 ± 0.1	-0.48 ± 0.15	2.16			
	B	2.28 ± 0.1	0.42 ± 0.1				
$^3Pb_2$					1.45 ± 0.10 [a] 1.366 ± 0.01 [b]	1.53	0.41
$^1Pb_3^-$	X	1.68 ± 0.1	-0.45 ± 0.1	1.89			0.30
	A	2.31 ± 0.1	-0.16 ± 0.1	2.19			
$^2Pb_3$					1.700 ± 0.088 [a] 1.45	1.84	0.58
$^2Pb_4^-$	X	1.58 ± 0.1	-0.55 ± 0.1	1.66			0.60
	A	2.23 ± 0.1	0.027 ± 0.1	2.68			
$^1Pb_4$					1.550 ± 0.088 [a] 1.370 ± 0.030 [c]	1.65	1.14

[a]Reference 23.
[b]Reference 25.
[c]Reference 24.

gies were also reported to a triplet $^3\Pi_u$ (1_u) and singlet $^1\Delta_g (2_g)$ electronic states. In our case, we calculated a transition to a singlet state resulting from the HOMO-1 at an energy of 2.16 eV, in good agreement with the observed band B of 2.28 ± 0.1 eV.

The Pb_3^- cluster has a stable atomic structure and slightly higher detachment energy than those of the dimer and tetramer. The electronic band X in the photoelectron image of the Pb_3^- cluster exhibits a preferential perpendicular angular distribution consistent with p-orbital detachment at low to medium energies. The HOMO has B_2 symmetry and is mostly composed of p orbitals. The photodetachment in the A transition in the Pb_3^- cluster results from an orbital of similar symmetry and composition than that for the X transition. However, in transition A the detachment occurs near the threshold where an isotropic angular distribution is predominant. The electronic affinities of Pb_2 and Pb_4 are close in value, 1.366 ± 0.01 (Ref. 25) and 1.37 ± 0.03,[24] respectively. The transition X in the Pb_4^- cluster has partially perpendicular distribution relative to the polarization direction. The photoelectron detachment occurs from a HOMO of B_{1g} symmetry mainly formed from a p orbital. Transition A results from the HOMO-1 of B_{2u} symmetry and shows isotropic angular distribution due to the low kinetic energy of the detached electrons. In summary, the photoelectron angular distributions in Pb_n clusters are dependent on both the kinetic energy of the detached electrons and the symmetry of the orbital, where a perpendicular distribution occurs at intermediate kinetic energies while parallel and isotropic distributions are dominant at high and near threshold detachment energies, respectively.

The optimized geometries of the ground states of the anionic and neutral Pb_n with $n=2-4$ series are shown in Fig. 9. The Pb_2 dimer is optimized to a triplet state configuration with a bond length of 2.94 Å. The Pb_3 cluster also in a triplet state exhibits an equilateral-triangle geometry (D_{3h}) with side bond length of 3.03 Å. These results are in good agreement with the DFT GGA study of Rajesh *et al.*[46] and with the results reported by Balasubramanian *et al.*[56] using the

CASSCF and MRSDCI methods for Pb_3. The Pb_4 cluster in a singlet state adopted a planar rhombus geometry (D_{2h}) with a Pb–Pb distance of 3.02 Å, similar to that calculated by Rajesh *et al.*[46] All the anionic Pb_n^- ($n=2-4$) clusters are optimized to doublet spin states with similar geometries to those of the respective neutral Pb_n, but in general with shorter Pb-Pb bond lengths. Pb_3^- is optimized to an isosceles (C_{2v}) triangle, while Pb_4^- presented D_{2h} symmetry.

IV. CONCLUSIONS

In this study, we reported the results of photoelectron imaging experiments of negatively charged bimetallic Bi_mGa_n and Pb_n clusters using photons of 527 nm wavelength. The $BiGa_n$ clusters show higher EAs with increasing number of Ga atoms from $n=0$ to $n=2$, while the photoelectron images of Pb_n with $n=1-4$ exhibit significant variation in the photoelectron angular distributions with the change in the cluster size. The anisotropy parameters of the Bi_mGa_n and Pb_n clusters were found to be dependent on both the orbital symmetry and electron kinetic energies. The optimized atomic structures for the anion and neutral Bi_mGa_n clusters were shown to exhibit the lowest possible multiplicity, sin-
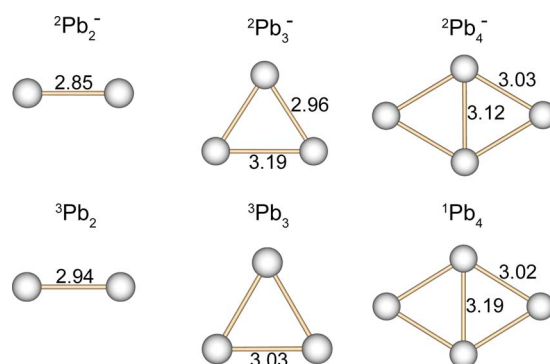

FIG. 9. (Color online) Optimized geometries of $Pb_n (n=2-4)$ anionic and neutral clusters. Bond lengths are given in angstroms and the superscripts indicate spin multiplicity.

glet and doublet for the even and odd electron systems, respectively, with the exception of BiGa which has a triplet ground state.

From the analysis of ΔE_{Ga} and the EAs, we found that the $BiGa_2^-$, $Bi_2Ga_3^-$ and $Bi_2Ga_5^-$ anionic, and $BiGa_3$, $BiGa_5$, Bi_2Ga_4, and Bi_2Ga_6 neutral clusters are quite stable. The stability of the anionic and neutral Bi_2Ga_n clusters is attributed to an even-odd effect, with clusters having an even number of electrons also displaying larger HOMO-LUMO gaps. The stability of the neutral $BiGa_3$ cluster is rationalized as being similar to $BiAl_3$, an all-metal aromatic cluster.

ACKNOWLEDGMENTS

[1] A. W. Castleman and K. H. Bowen, J. Phys. Chem. **100**, 12911 (1996).
[2] A. Sanov and W. C. Lineberger, Phys. Chem. Chem. Phys. **6**, 2018 (2004).
[3] *Clusters of Atoms and Molecules I, II*, edited by H. Haberland (Springer, Berlin, 1994).
[4] Q. Phenomena, in *Clusters and Nanostructures*, edited by S. N. Khanna and A. W. Castleman, Jr. (Springer, Berlin, 2003).
[5] P. Jena and A. W. Castleman, Jr., Proc. Natl. Acad. Sci. U.S.A. **103**, 10560 (2006).
[6] I. Vurgaftman, J. R. Meyer, and L. R. Ram-Mohan, J. Appl. Phys. **89**, 5815 (2001).
[7] Y. Liu, Q. L. Zhang, F. K. Tittel, R. F. Curl, and R. E. Smalley, J. Chem. Phys. **85**, 7434 (1986).
[8] M. A. Allaham and K. Raghavachari, Chem. Phys. Lett. **187**, 13 (1991).
[9] M. L. Polak, J. Ho, G. Gerber, and W. C. Lineberger, J. Chem. Phys. **95**, 3053 (1991).
[10] W. Andreoni, Phys. Rev. B **45**, 4203 (1992).
[11] K. R. Asmis, T. R. Taylor, and D. M. Neumark, Chem. Phys. Lett. **308**, 347 (1999).
[12] H. H. Kwong, Y. P. Feng, and T. B. Boo, Comput. Phys. Commun. **142**, 290 (2001).
[13] X. L. Zhou, J. J. Zhao, X. S. Chen, W. Lu, R. H. Xie, Z. F. Chen, and R. B. King, J. Comput. Theor. Nanosci. **5**, 70 (2008).
[14] M. D. Morse, in *Advances in Metal and Semiconductor Clusters*, edited by M. A. Duncan (JAI, Connecticut, 1993), Vol. 1.
[15] J. C. Phillips, J. Chem. Phys. **87**, 1712 (1987).
[16] M. E. Geusic, M. F. Jarrold, and R. R. Freeman, J. Chem. Phys. **84**, 2421 (1986).
[17] H. W. Kroto, J. R. Heath, S. C. O'Brien, R. F. Carl, and R. E. Smalley, Nature (London) **318**, 162 (1985).
[18] J. C. Phillips, Chem. Rev. **86**, 619 (1986).
[19] N. E. Christensen, S. Satpathy, and Z. Pawlowska, Phys. Rev. B **34**, 5977 (1986).
[20] P. C. Engelking and W. C. Lineberger, Phys. Rev. A **19**, 149 (1979).
[21] E. Surber and A. Sanov, J. Chem. Phys. **116**, 5921 (2002); A. V. Davis,

[22] R. Wester, A. E. Bragg, and D. M. Neumark, *ibid.* **118**, 999 (2003).
[22] R. Mabbs, E. Surber, L. Velarde, and A. Sanov, J. Chem. Phys. **120**, 5148 (2004).
[23] G. Ganteför, M. Gausa, K. H. Meiwes-Broer, and H. O. Lutz, Z. Phys. D: At., Mol. Clusters **12**, 405 (1989).
[24] Y. Negishi, H. Kawamata, A. Nakajima, and K. Kaya, J. Electron Spectrosc. Relat. Phenom. **106**, 117 (2000).
[25] J. Ho, M. L. Polak, and W. C. Lineberg, J. Chem. Phys. **96**, 144 (1992).
[26] M. A. Sobhy and A. W. Castleman, Jr., J. Chem. Phys. **126**, 154314 (2007).
[27] W. C. Wiley and I. H. McLaren, Rev. Sci. Instrum. **26**, 1150 (1955).
[28] K. Pichugin, E. Grumbling, L. Velarde, and A. Sanov, J. Chem. Phys. **129**, 044311 (2008).
[29] V. Dribinski, A. Ossadtchi, V. A. Mandelshtam, and H. Reisler, Rev. Sci. Instrum. **73**, 2634 (2002).
[30] S. M. Sheehan, G. Meloni, B. F. Parsons, N. Wehres, and D. M. Neumark, J. Chem. Phys. **124**, 064303 (2006).
[31] J. P. Perdew, K. Burke, and M. Ernzerhof, Phys. Rev. Lett. **77**, 3865 (1996).
[32] A. M. Köster, P. Calaminici, M. E. Casida, R. Flores-Moreno, G. Geudtner, A. Goursot, T. Heine, A. Ipatov, F. Janetzko, J. M. del Campo, S. Patchkovskii, J. U. Reveles, D. R. Salahub, and A. Vela, DEMON2K, version 2.3.6, the deMon Developers, Cinvestav, México, available at www.deMon-software.com.
[33] P. Calaminici, F. Janetzko, A. M. Köster, R. Mejia-Olvera, and B. Zuñiga-Gutierrez, J. Chem. Phys. **126**, 044108 (2007).
[34] B. Metz, H. Stoll, and M. Dolg, J. Chem. Phys. **113**, 2563 (2000).
[35] K. A. Peterson, J. Chem. Phys. **119**, 11099 (2003).
[36] J. U. Reveles and A. M. Köster, J. Comput. Chem. **25**, 1109 (2004).
[37] E. Keller, Chem. Unserer Zeit **14**, 56 (1980).
[38] P. Flükiger, H. P. Lüthi, S. Portmann, and J. Weber, *Molekel 4.0, Swiss National Supercomputing Centre CSCS* (Manno, Switzerland, 2000).
[39] H. Hotop and W. C. Lineberger, J. Phys. Chem. Ref. Data **14**, 731 (1985); W. W. Williams, D. L. Carpenter, A. M. Covington, M. C. Koepnick, D. Calabrese, and J. S. Thompson, J. Phys. B **31**, L341 (1998).
[40] R. C. Bilodeau and H. K. Haugen, Phys. Rev. A **6402**, 4501 (2001).
[41] K. P. Huber and G. Herzberg, *Molecular Spectra and Molecular Structure IV Constants of Diatomic Molecules* (Van Nostrand Reinhold, New York, 1979).
[42] Y. L. Luo, *Comprehensive Handbook of Chemical Bond Energies* (CRN, Boca Raton, Florida, 2007).
[43] S. Kurth, J. P. Perdew, and P. Blaha, Int. J. Quantum Chem. **75**, 889 (1999).
[44] Y. Zhao, W. Xu, Q. Li, Y. Xie, and H. F. Schaefer III, J. Phys. Chem. A **108**, 7448 (2004).
[45] B. Song and P. L. Cao, J. Chem. Phys. **123**, 144312 (2005).
[46] C. Rajesh, C. Majumder, M. G. R. Rajan, and S. K. Kulshreshtha, Phys. Rev. B **72**, 235411 (2005).
[47] U. Gupta, J. U. Reveles, J. J. Melko, S. N. Khanna, and A. W. Castleman, Jr., Chem. Phys. Lett. **467**, 223 (2009).
[48] K. Balasubramanian and D. W. Liao, J. Chem. Phys. **95**, 3064 (1991).
[49] See EPAPS Document No. E-JCPSA6-130-002905 for the tables listing the calculated Ga energy gains (ΔE_{Ga}) and HOMO-LUMO gaps of the anion and neutral Bi_mGa_n clusters, calculated adiabatic EAs, and VDEs for both the $BiGa_n$ $n=1-6$ and Bi_2Ga_n $n=1-6$ series, and the corresponding HOMO-LUMO gaps, and three figures that depict the one electron energy levels and charge densities of the orbitals of Bi and the molecular orbitals of the $BiGa_2^-$, Ga_2^-, $BiGa_3$, Ga_3, and $BiGa_5$ clusters. For more information on EPAPS, see http://www.aip.org/pubservs/epaps.html.
[50] C. E. Jones, Jr., P. A. Clayborne, J. U. Reveles, J. J. Melko, U. Gupta, S. N. Khanna, and A. W. Castleman, Jr., J. Phys. Chem. A **112**, 13316 (2008).
[51] C. S. Xu, E. Debeer, D. W. Arnold, C. C. Arnold, and D. M. Neumark, J. Chem. Phys. **101**, 5406 (1994).
[52] T. R. Taylor, H. Gomez, K. R. Asmis, and D. M. Neumark, J. Chem. Phys. **115**, 4620 (2001).
[53] T. R. Taylor, K. R. Asmis, H. Gomez, and D. M. Neumark, Eur. Phys. J. D **9**, 317 (1999).
[54] D. Hanstorp, C. Bengtsson, and D. J. Larson, Phys. Rev. A **40**, 670 (1989).
[55] K. Balasubramanian and K. S. Pitzer, J. Chem. Phys. **78**, 321 (1983).
[56] K. Balasubramanian and D. Majumdar, J. Chem. Phys. **115**, 8795 (2001).